Computational Materials Science 83 (2014) 457–462

Contents lists available at ScienceDirect

Computational Materials Science

journal homepage: www.elsevier.com/locate/commatsci

Mechanical properties and atomistic deformation mechanism of spinel-type BeP_2N_4

Meiguang Zhang [a,*], Haiyan Yan [b], Yaru Zhao [a], Qun Wei [c,*]

[a] Department of Physics and Information Technology, Nonlinear Research Institute, Baoji University of Arts and Sciences, Baoji 721016, China
[b] College of Chemistry and Chemical Engineering, Baoji University of Arts and Sciences, Baoji 721013, China
[c] School of Physics and Optoelectronic Engineering, Xidian University, Xi'an 710071, China

ARTICLE INFO

Article history:
Received 20 August 2013
Received in revised form 7 October 2013
Accepted 24 November 2013

Keywords:
Beryllium phosphorus nitride
Anisotropic mechanical properties
Ideal shear strength
First-principles calculations

ABSTRACT

The anisotropic mechanical properties and atomistic deformation mechanism of incompressible γ-BeP_2N_4 were comprehensively investigated by first-principles calculations. According to the dependence of the Young's modulus on different directions in crystal, the γ-BeP_2N_4 exhibits a well-pronounced anisotropy which may impose certain limitations and restrictions on its applications. The ideal strength calculations demonstrated that γ-BeP_2N_4 shows substantially lower ideal shear strength than superhard *c*-BN and diamond, suggesting that it cannot be intrinsically superhard as claimed in the previous studies. Furthermore, the origin of the lattice instability of γ-BeP_2N_4 under large shear strain that occurs at the atomic level during plastic deformation can be attributed to the breaking of P–N bonds in PN_6 octahedrons.

Crown Copyright © 2013 Published by Elsevier B.V. All rights reserved.

1. Introduction

The quest for intrinsic superhard materials is motivated by scientific curiosity and by the need of materials with high hardness, high thermal stability, and oxidation resistance [1,2]. In synthesizing intrinsic strongly covalent superhard materials formed by the light elements (boron, carbon, nitrogen, etc.) [3–6], one of the lightest elements beryllium (Be) has been often neglected in this field. However, Kaner et al. [7] recently pointed out that the compounds of Be with other light elements may form alternative superhard materials. The following theoretical calculations [8–10] indeed found that $B_{12}N_2Be$ and Be_3N_2 are potential superhard materials with the calculated hardness of about 50 GPa. A novel beryllium phosphorus nitride BeP_2N_4 with phenakite-type structure (hereafter denoted as β-BeP_2N_4), recently has been experimentally determined by Pucher et al. [11] under high temperature and high pressure. Experimental and theoretical works [11–13] have found that β-BeP_2N_4 is isotypic and isoelectronic to β-Si_3N_4, which can transform into cubic spinel-type γ-Si_3N_4 at pressure of 15 GPa [14,15]. It is well known that ceramics made up of Si_3N_4 cover a broad range of applications. Predominant materials properties of this compound are chemical inertness, high hardness, mechanical strength, etc. Especially for γ-Si_3N_4, the measured Vickers hardness is between 35 GPa [16] and 43 GPa [17,18] and confirms that this material qualifies as a potentially superhard solid. Meanwhile, in the γ-Si_3N_4, octahedrally and tetrahedrally coordinated Si atoms are fixed by symmetry and the N positions possess a single degree of freedom in support of the suggestion that a small number of internal degrees of freedom are necessary but not sufficient condition for a superhard material [19]. The successful synthesis of γ-Si_3N_4 has evoked a search for other isoelectronic or isostructural compounds with comparable materials properties. Accordingly, as the isoelectronic compound β-BeP_2N_4 which under pressure might also form a spinel-type phase (hereafter denoted as γ-BeP_2N_4) with interesting properties as well.

Most recently, different density functional theory calculations [11–13] have supported the possible existence of the γ-BeP_2N_4 at readily attainable pressures (15–24 GPa) by state-of-the-art high pressure techniques. The calculations of mechanical properties further indicated that the γ-BeP_2N_4 is a promising ultra-incompressible material with notably large elastic moduli. Using two different empirical and semi-empirical models proposed by Sung and Sung [20] and Gao et al. [21], Ding and Xiao [13] estimated the hardness of the γ-BeP_2N_4 to be 43.3–45.2 GPa. Therefore, it seems as if the recent theoretical studies [11–13] have reached a consensus that γ-BeP_2N_4 can be qualified as a superhard material. However, a predictability of hardness [20–22] from the equilibrium properties (such as bulk or shear modulus, bond length, charge density, ionicity, etc.) is very limited because plastic deformation of materials occurs far from equilibrium upon bond breaking in practical measurement of hardness. More importantly, studies of the stress–strain relations and the underlying atomistic bond-breaking processes can provide important insights into the

* Corresponding authors. Tel./fax: +86 917 3364258.
E-mail addresses: zhmgbj@126.com (M. Zhang), weiaqun@163.com (Q. Wei).

0927-0256/$ - see front matter Crown Copyright © 2013 Published by Elsevier B.V. All rights reserved.
http://dx.doi.org/10.1016/j.commatsci.2013.11.044

fundamental aspects of the deformation and failure modes critical to the understanding of the mechanical behavior, especially for hardness [1,2]. Previous studies [23,24] have demonstrated that ultimate hardness of a material may be assessed from its ideal shear strength and bonding nature, which also appears to correlate with the onset of dislocation formation in an ideal, defect-free crystal [25,26]. For example, ReB_2, which has been suggested to be superhard, undergoes a series of shear transitions and a final structural collapse [27]. Therefore, first-principles studies on deformation and failure mode of the γ-BeP_2N_4 are highly desirable. In the present work, we have extended the mechanical properties of γ-BeP_2N_4 and presented in detail the variations of the elastic moduli along the arbitrary directions. The ideal strengths of the γ-BeP_2N_4 in comparison with γ-Si_3N_4 were systematically studied in order to provide a deeper insight into mechanical behavior and hardness.

2. Computational methods

First-principles calculations were performed using the VASP code [28] with the generalized-gradient approximation (GGA) proposed by Perdew–Burke–Ernzerhof exchange–correlation functional [29]. The electron and core interactions were included by using the frozen-core all-electron projector augmented wave (PAW) potential [30]. Tests of the computational parameters showed that converged results of the Kohn–Sham equations can be obtained with a plane-wave energy cutoff of 600 eV and a proper Monkhorst–Pack grid ($10 \times 10 \times 10$) [31] in the Brillouin zone. During the geometrical optimization, all forces on atoms were converged to less than 0.001 eV/Å and the total stress tensor was reduced to the order of 0.01 GPa. Dynamical properties were calculated within the harmonic approximation [32] by using the direct method based on the forces calculated via the Hellmann–Feynman theorem. The stress–strain relationships were calculated by incrementally deforming the model cell in the direction of the applied strain, and simultaneously relaxing the cell basis vectors conjugated to the applied strain, as well as the positions of atoms inside the cell, at each step [24,33]. To ensure that the strain path is continuous, the starting position at each strain step has been taken from the relaxed coordinates of the previous strain step.

3. Results and discussion

The crystal structure of γ-BeP_2N_4 is sketched in Fig. 1a, in which two basic building blocks along $\langle 100 \rangle$ directions are edge-shared PN_6 octahedrons and BeN_4 tetrahedrons. The equilibrium structural parameter for γ-BeP_2N_4 [space group: $Fd\bar{3}m$ (No. 227)] was obtained by full relaxations of both lattice constant and internal atomic coordination. The optimized lattice constant for γ-BeP_2N_4 is $a = 7.553$ Å, which is in good agreement with other theoretical values $a = 7.564$ Å [11], 7.4654 Å [12], and 7.471 Å [13]. The calculated bond lengths for P–N (1.819 Å) and Be–N (1.759 Å) in γ-BeP_2N_4 also agree well with these available theoretical results. Moreover, the total energy of γ-BeP_2N_4 is calculated by varying the volume and these calculated E–V data are fitted using the Birch–Murnaghan equation of state (EOS) [34]. The obtained bulk modulus B_0 and its pressure derivative are 265 GPa and 3.99, which are consistent with the theoretical values of 268 GPa and 4.036 [13], thus confirming the reliability of the present calculations. At zero temperature a stable crystalline structure requires all phonon frequencies to be positive. We have calculated the phonon dispersion curves of the γ-BeP_2N_4 at 0 GPa. No imaginary phonon frequencies are found in the whole Brillouin zones (Fig. 1b), indicating the dynamical stability of this spinel-type structure. The similar case has been reported for the high-pressure polymorphs of γ-Si_3N_4 typically synthesized at high pressure and high temperature, turned out to be quenchable at ambient pressure to at least 700 K [14].

The elastic stabilities, incompressibility, and rigidity of both γ-BeP_2N_4 and γ-Si_3N_4 are determined from the calculated elastic constants by applying a set of given strains with a finite variation. Table 1 summarizes the calculated single-crystal elastic constants C_{ij} and derived Hill elastic moduli of γ-BeP_2N_4 and γ-Si_3N_4 along with previous experimental and theoretical results [11–13,18,19,35–37]. One can see that the obtained elastic constants C_{ij} and derived Hill elastic moduli [38] of γ-BeP_2N_4 are very close to those of γ-Si_3N_4, which agree well with available experimental data [18,35,36]. The agreement of γ-Si_3N_4 supports the reliability of the elastic calculations for γ-BeP_2N_4 although there are no available experimental data for comparison. Furthermore, our calculated elastic constants C_{ij} and derived Hill elastic moduli of γ-BeP_2N_4 listed in Table 1 are in a good accordant with the results reported in Refs. [13,11] using the same GGA+PAW approach, but smaller than those recorded in Ref. [12] using a slightly different approach [the orthogonalized linear combination of atomic orbitals (OLCAO) method]. The mechanical stabilities of both γ-BeP_2N_4 and γ-Si_3N_4 satisfy the Born–Huang criterion [39] for a cubic crystal [$C_{11} - |C_{12}| > 0$, $C_{11} > 0$, $C_{44} > 0$, $C_{11} + 2C_{12} > 0$], indicating that both compounds are mechanically stable at ambient conditions. A well-established consideration of whether a crystalline solid is intrinsically ductile or brittle is if dislocation embryos can be nucleated from an atomically sharp crack prior to its propagation by cleavage [40,41]. This bifurcation in mechanical behavior is characterized by the ratio (specific to the solid) of the shear

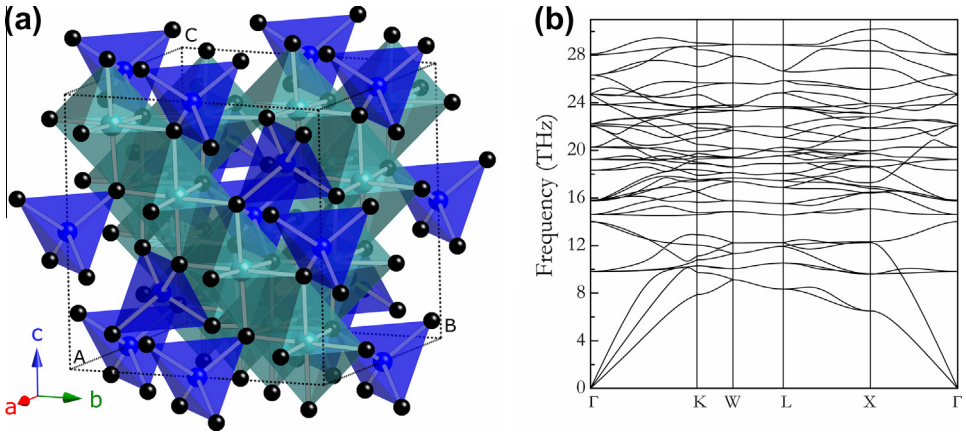

Fig. 1. Crystal structure of γ-BeP_2N_4, the blue, black, and gray spheres represent Be, N, and P atoms, respectively (a), and phonon dispersion curves of γ-BeP_2N_4 at 0 GPa (b). (For interpretation of the references to colour in this figure legend, the reader is referred to the web version of this article.)

Table 1
Calculated Elastic Constants C_{ij}, Bulk Modulus B, Shear Modulus G, Young's Modulus E, and ideal strength (minimum tensile strength σ_{min} and shear strength τ_{min}) (in units of GPa). Also shown is G/B ratio.

Compound	Source	C_{11}	C_{12}	C_{44}	B	G	E	G/B	σ_{min}	τ_{min}
γ-BeP_2N_4	Present	510	146	318	268	254	579	0.951	$\sigma_{\langle 100\rangle}$ = 42.5	$\tau_{(1\,1\,0)\langle 1\,\bar{1}\,0\rangle}$ = 35.2
	Theory [13]	532	147	335	275	268	607	0.980		
	Theory [12]	643	98	221	279	231	544			
	Theory [11]				263					
γ-Si_3N_4	Present	520	181	326	294	250	585	0.851	$\sigma_{\langle 110\rangle}$ = 41.2	$\tau_{(1\,1\,1)\langle \bar{1}\,\bar{1}\,2\rangle}$ = 31.3
	Exp. [18]				290 (5)					
	Exp. [35]				300 (10)					
	Exp. [36]				308					
	Theory [19]	511	174	323	286					
	Theory [37]	500	159	334	273					
	Theory [35]	533	191	341	305	258				
c-BN	Theory [45]	786	172	445	376	390			$\sigma_{\langle 111\rangle}$= 55.3	$\tau_{(1\,1\,1)\langle 1\bar{1}2\rangle}$= 58.3
Diamond	Theory [46]	1079	124	578	442	528			$\sigma_{\langle 111\rangle}$= 82.3	$\tau_{(111)\langle \bar{1}\,\bar{1}\,2\rangle}$= 86.6

modulus to the bulk modulus, i.e., G/B, by simply considering G as the resistance to plastic deformation and B the resistance to fracture. The critical G/B ratio which separates ductile and brittle materials is around 0.57 [42], i.e., if G/B <0.57 the material behaves in a ductile manner, otherwise the material behaves in a brittle manner. As shown in Table 1, the calculated G/B ratios for γ-BeP_2N_4 and γ-Si_3N_4 (0.951 and 0.851) suggest their brittle behaviors. A useful visualization of the elastic anisotropy can be obtained by plotting three-dimensional picture of dependence of the Young's modulus E on a direction in crystal. For cubic solid, it is described by the following [43]:

$$E^{-1} = s_{11} - \beta_1(\alpha^2\beta^2 + \alpha^2\gamma^2 + \beta^2\gamma^2) \quad (1)$$

where α, β, and γ is the direction cosine of the tensile stress direction, $\beta_1 = 2s_{11} - 2s_{12} - s_{44}$, and s_{11}, s_{12}, and s_{44}, are elastic compliance constants which are given by Ney [44]. This equation determines a three-dimensional closed surface, and the distance from the origin of system of coordinate to this surface equals to the Young's modulus in a given direction. For a perfectly isotropic medium this surface would be a sphere. Fig. 2a and b show well-pronounced anisotropy for γ-BeP_2N_4 and γ-Si_3N_4, and the cross-sections of γ-BeP_2N_4 and γ-Si_3N_4 in the bc plane are also shown in Fig. 2c and d for comparison. Analytical equations for determination of the maximum and minimum values of the Young's moduli are [43] $E_{max} = 1/s_{11}$ and $E_{min} = 3/(s_{11} + 2s_{12} + s_{44})$ if $\beta_1 < 0$. The "max" and "min" subscripts should be interchanged if $\beta_1 > 0$. For γ-BeP_2N_4 (γ-Si_3N_4), the estimated E_{max} and E_{min} values are 802(882) GPa along [1 0 0] directions and 556(554) GPa along [1 1 1] directions, respectively. The ratio E_{max}/E_{min} of γ-BeP_2N_4 (1.442) is smaller than that of γ-Si_3N_4 (1.592), indicating that there is a larger elastic anisotropy in γ-Si_3N_4.

The ideal strength in a specified direction is microscopically determined by bond strength and breaking nature under strain. The stress–strain relations upon tension and shear for the cubic spinel-type phase are calculated in three main crystallographic

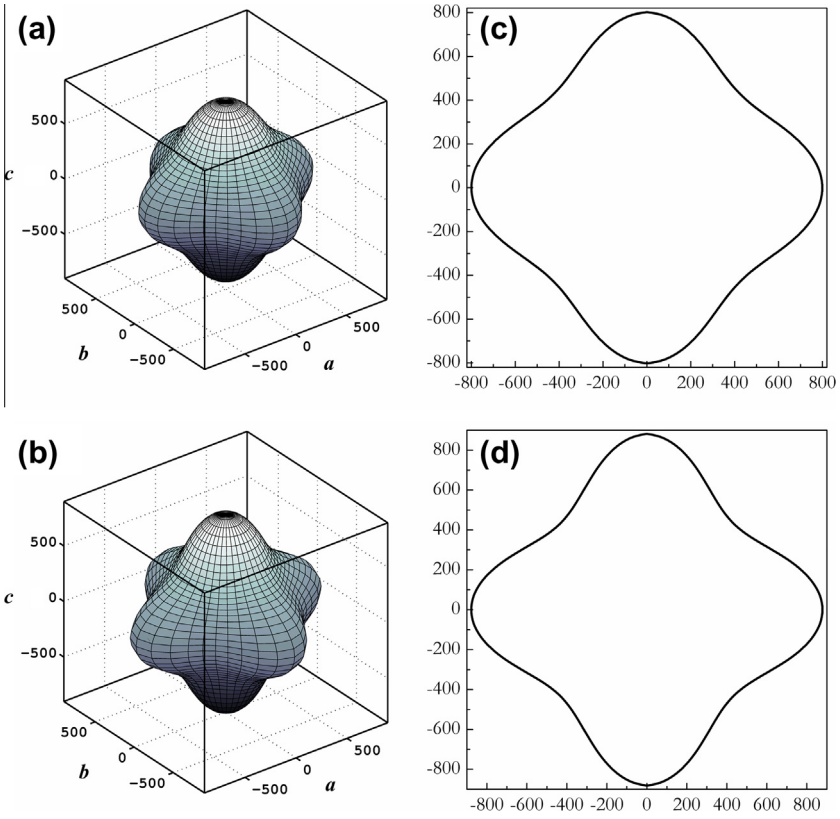

Fig. 2. Directional dependence of the Young's Modulus E for γ-BeP_2N_4 (a) and γ-Si_3N_4 (b), the corresponding projection in bc plane for γ-BeP_2N_4 (c) and γ-Si_3N_4 (d).

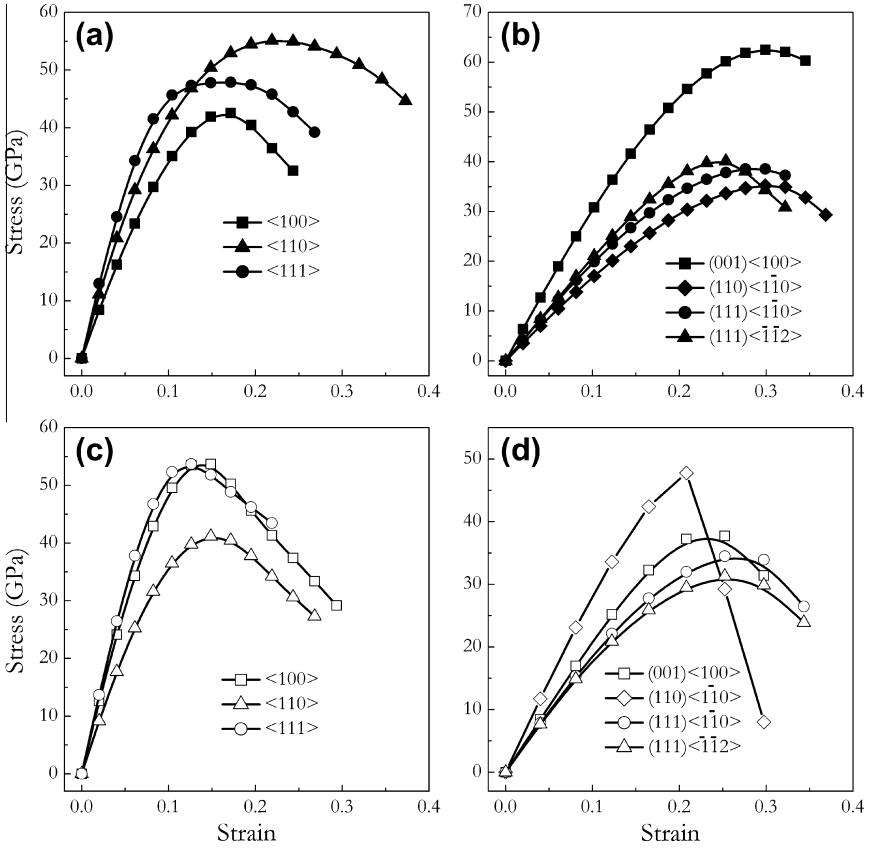

Fig. 3. Calculated stress–strain relations for γ-BeP_2N_4 in various tensile (a) and shear (b) directions, and for γ-Si_3N_4 in various tensile (c) and shear (d) directions.

directions through projection of an 56-atom unit cell onto the corresponding crystal axes with one axis parallel to the strain direction for tension deformation, or with one axis parallel to the slip direction and another axis perpendicular to the slip plane for shear deformation. The anisotropic ideal strengths of both γ-BeP_2N_4 and γ-Si_3N_4 were deduced from the stress–strain relationships, which are shown in Fig. 3 and summarized in Table 1, together with those of superhard *c*-BN [45] and diamond [46] for comparisons. Firstly, under tension, the anisotropic ratio for γ-BeP_2N_4 (Fig. 3a) is about 1:1.28:1.08 (the ideal decohesion strengths are $\sigma_{\langle 100\rangle}$ = 42.5 GPa, $\sigma_{\langle 110\rangle}$ = 54.5 GPa, $\sigma_{\langle 111\rangle}$ = 45.8 GPa) which is close to that of γ-Si_3N_4 (Fig. 3c) of 1:1.3:1 ($\sigma_{\langle 100\rangle}$ = 53.7 GPa, $\sigma_{\langle 110\rangle}$ = 41.2 GPa, $\sigma_{\langle 111\rangle}$ = 53.7 GPa). For γ-BeP_2N_4 (Table 1), the weakest direction along $\langle 100\rangle$ with ideal tensile strength of 42.5 GPa is slightly lower than the lowest tensile strength of 55.3 GPa for *c*-BN along the $\langle 111\rangle$ direction [45]. This, however, does not suggest its intrinsically superhard character. Because plastic deformation occurs in shear, one has to compare the calculated ideal shear strengths and the bonding nature. Secondly, the lowest shear strength for γ-BeP_2N_4 (see Table 1 and Fig. 3b) found in the $(110)\langle 1\bar{1}0\rangle$ slip system is 35.2 GPa, which is about 40% lower than the lowest shear strength of 58.3 GPa in *c*-BN [45], showing its lower shear resistance or potential superhardness. This is the similar case for γ-Si_3N_4 presented in Table 1 and Fig. 3d. In spite of their significantly high bulk moduli, both γ-BeP_2N_4 and γ-Si_3N_4 are much weaker than *c*-BN and diamond in terms of shear moduli and strengths. Thus, higher incompressibility does not necessarily guarantee higher shear resistance and hardness. Thirdly, the lowest shear strength of γ-BeP_2N_4 along the $(110)\langle 1\bar{1}0\rangle$ direction (35.2 GPa), is lower than the lowest tensile strength (42.5 GPa). This means the failure mode in γ-BeP_2N_4 is dominated by the shear type. To shed light on the origin of deformation mechanism in this direction, the variations of bond lengths as a function of applied strain under $(110)\langle 1\bar{1}0\rangle$ direction were plotted in Fig. 4. At equilibrium state as mentioned above, the P–N bond length ($d1 = d2 = d3$) in PN_6 octahedrons and Be–N bond length in BeN_4 tetrahedrons [see the inset (c) in Fig. 4] is 1.819 Å and 1.759 Å, respectively. Under increasing shear strains, the P–N bonds denoted as $d1$ in PN_6 octahedrons are stretched and break at the critical shear strain of γ = 0.2990, which limits the achievable strengths of γ-BeP_2N_4. Such a bond-breaking can also be clearly seen from the selected crystal structures before (γ = 0.2762) and after (γ = 0.3219) shear

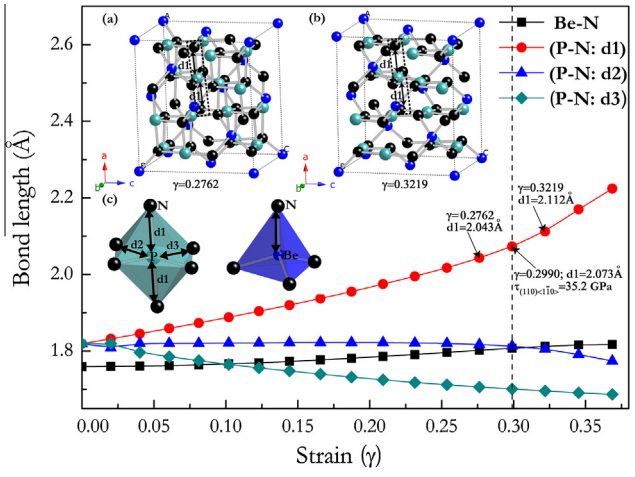

Fig. 4. Calculated bond lengths as a function of strain for γ-BeP_2N_4 under shear deformation along $(110)\langle 1\bar{1}0\rangle$ directions. Insets: crystal structures before (a) and after (b) shear instability, and basic building blocks of PN_6 octahedrons and BeN_4 tetrahedrons in γ-BeP_2N_4 (c). The dashed line represents the shear-induced structural deformation firstly occurrence.

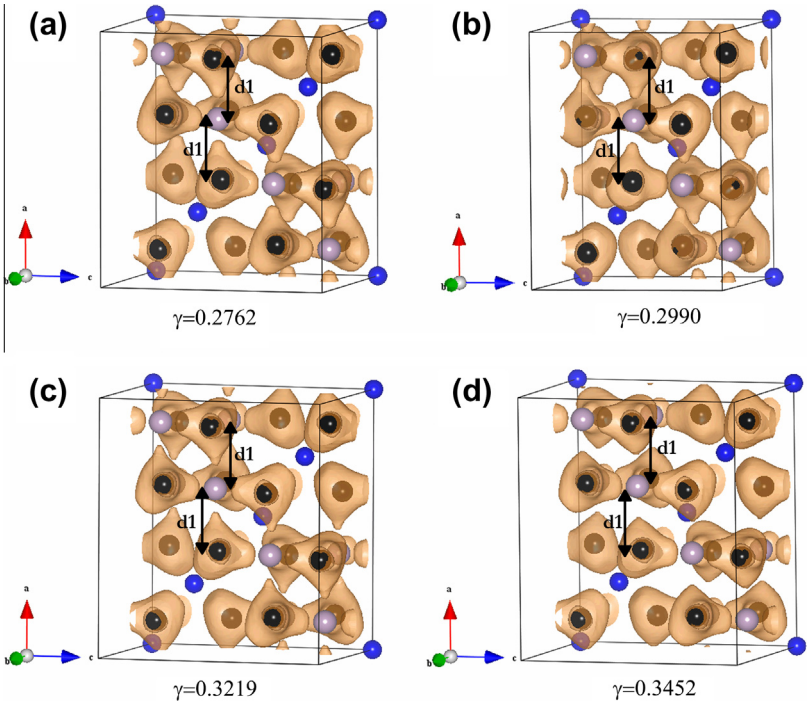

Fig. 5. Developments of ELF for γ-BeP_2N_4 during shear in the $(1\,1\,0)\langle 1\,\bar{1}\,0\rangle$ slip at different strains of 0.2762 (a), 0.2990 (b), 0.3219 (c), and 0.3452 (d).

instability [see the inset (a) and insect (b) in Fig. 4]. It means that this shear-induced structural deformation firstly occur at strain of $\gamma = 0.2990$ through the collapse of PN_6 octahedrons by simultaneously breaking of $d1$ bonds, resulting in the formation of puckered P–N layers. The bond length of $d2$ remains nearly invariant up to the critical strain of 0.2990 and then decreases abruptly along with the breaking of $d1$ bonds. The P–N bond indicated as $d3$ decreases slowly in the whole studied strain range, on the contrary, all the Be–N bonds in BeN_4 tetrahedrons increase conformably at each strain. Therefore, the instability of P–N bonds under shear deformation for γ-BeP_2N_4 can be attributed to a local transformation of sp^3 to sp^2 upon the shear. In addition, the changes of the Electronic Localization Function (ELF) of γ-BeP_2N_4 upon shear deformation [$(1\,1\,0)\langle 1\,\bar{1}\,0\rangle$ direction] were analyzed to rationalize the deformation of $d1$ bonds. At ELF = 0.7, Fig. 5 presents the electron localization distributions of γ-BeP_2N_4 at different strains of about 0.2762, 0.2990, 0.3219, and 0.3452, i.e. before and after the instability for the $(1\,1\,0)\langle 1\,\bar{1}\,0\rangle$ slip system (see Fig. 3b). It can be seen that at strains of 0.2762 and 0.2990 (before the shear instability) the ELF are similar, but a significant difference appears around the N and P atoms for N and P at large strains of 0.3219 and 0.3452 (after the shear instability). Especially for ELF at strain of 0.3452 (Fig. 5d), the charge density between N and P atom is nearly centered on the N atom, i.e. the $d1$ bonding becomes rather weak at this large shear strain. On the basis of these calculations, the results highlight the importance of bonding deformation mechanism in the design of and search for intrinsically hard or superhard materials.

4. Conclusions

In summary, we have carried out first-principles calculations on structural and mechanical properties as well as ideal strengths for recently proposed γ-BeP_2N_4. The calculated equilibrium lattice parameters, bulk modulus, and its pressure derivative are consistent with previous theoretical results. The orientation dependence of the Young's modulus reveals that the γ-BeP_2N_4 is the stiffest along [1 0 0] and the most compliant along [1 1 1] in response to tension or compression loading. The substantially low shear strength of γ-BeP_2N_4 indicates that it cannot be intrinsically superhard. Detailed analyses of the deformed atomic structures under shear strain reveal that the lattice instability of γ-BeP_2N_4 is due to the collapse of PN_6 octahedrons by simultaneously breaking of $d1$ bonds which limits its achievable strength.

Acknowledgments

This work was supported by the National Natural Science Foundation of China (Grant No. 11204007), the Natural Science Basic Research plan in Shaanxi Province of China (Grant No. 2012JQ1005, 2013JQ1007), Education Committee Natural Science Foundation in Shaanxi Province of China (Grant No. 2013JK0638), and the Fundamental Research Funds for the Central Universities.

References

[1] J. Haines, J.M. Leger, G. Bocquillon, Annu. Rev. Mater. Res. 31 (2001) 1.
[2] V.V. Brazhkin, A.G. Lyapin, R.J. Hemley, Philos. Mag. A 82 (2002) 231.
[3] F. Occelli, D.L. Farber, R.L. Toullec, Nat. Mater. 2 (2003) 151.
[4] J.C. Zheng, Phys. Rev. B 72 (2005) 052105.
[5] V.L. Solozhenko, D. Andrault, G. Fiquet, M. Mezouar, D.C. Fubie, Appl. Phys. Lett. 78 (2001) 1385.
[6] V.L. Solozhenko, O.O. Kurakevych, D. Andrault, Y.L. Gode, M. Mezouar, Phys. Rev. Lett. 102 (2009) 015506.
[7] R.B. Kaner, J.J. Gilman, S.H. Tolbert, Science 308 (2005) 126.
[8] H.Y. Gou, L. Hou, J.W. Zhang, G.F. Sun, L.H. Gao, F.M. Gao, Phys. Status Solidi B 245 (2008) 58.
[9] H.Y. Gou, L. Hou, J.W. Zhang, Z.B. Wang, L.H. Gao, F.M. Gao, Appl. Phys. Lett. 90 (2007) 191905.
[10] Y. Xia, Q. Li, Y.M. Ma, Comput. Mater. Sci. 49 (2010) S76.
[11] F.J. Pucher, S.R. Römer, F.W. Karau, W. Schnick, Chem. Eur. J. 16 (2010) 7208.
[12] W.Y. Ching, S. Aryal, P. Rulis, W. Schnick, Phys. Rev. B 83 (2011) 155109.
[13] Y.C. Ding, B. Xiao, Acta Phys. – Chim. Sin. 27 (2011) 1621.
[14] A. Zerr, G. Miehe, G. Serghiou, M. Schwarz, E. Kroke, R. Riedel, H. Fueß, P. Kroll, R. Boehler, Nature 400 (1999) 340.
[15] M. Schwarz, G. Miehe, A. Zerr, E. Kroke, B.T. Poe, H. Fuess, R. Riedel, Adv. Mater. 12 (2000) 883.

[16] J.Z. Jiang, F. Kragh, D.J. Frost, K. Ståhl, H. Lindelov, J. Phys.: Condens. Matter 13 (2001) L515.
[17] I. Tanaka, F. Oba, T. Sekine, E. Ito, A. Kubo, K. Tatsumi, H. Adachi, T. Yamamoto, J. Mater. Res. 17 (2002) 731.
[18] A. Zerr, M. Kempf, M. Schwarz, E. Kroke, M. Goken, R. Riedel, J. Am. Ceram. Soc. 85 (2002) 86.
[19] B. Kiefer, S.R. Shieh, T.S. Duffy, T. Sekine, Phys. Rev. B 72 (2005) 014102.
[20] C.M. Sung, M. Sung, Mater. Chem. Phys. 43 (1996) 1.
[21] F.M. Gao, J.L. He, E.D. Wu, S.M. Liu, D.L. Yu, D.C. Li, S.Y. Zhang, Y.J. Tian, Phys. Rev. Lett. 91 (2003) 015502.
[22] A. Šimůnek, J. Vackář, Phys. Rev. Lett. 96 (2006) 085501.
[23] Y. Zhang, H. Sun, C.F. Chen, Phys. Rev. Lett. 94 (2005) 145505.
[24] D. Roundy, C.R. Krenn, M.L. Cohen, J.W. Morris Jr., Phys. Rev. Lett. 82 (1999) 2713.
[25] Y. Umeno, Y. Kinoshita, T. Kitamura, Modell. Simuingl. Mater. Sci. Eng. 15 (2007) 27.
[26] J. Pokluda, M. Cerny, P. Sandera, M. Sob, J. Comput. – Aided Mater. Des. 11 (2004) 1.
[27] R.F. Zhang, D. Legut, R. Niewa, A.S. Argon, S. Veprek, Phys. Rev. B 82 (2010) 104104.
[28] G. Kresse, J. Furthmüller, Phys. Rev. B 54 (1996) 11169.
[29] J.P. Perdew, K. Burke, M. Ernzerhof, Phys. Rev. Lett. 77 (1996) 3865.
[30] G. Kresse, D. Joubert, Phys. Rev. B 59 (1999) 1758.
[31] H.J. Monkhorst, J.D. Pack, Phys. Rev. B 13 (1976) 5188.
[32] A. Togo, F. Oba, I. Tanaka, Phys. Rev. B 78 (2008) 134106.
[33] R.F. Zhang, S.H. Sheng, S. Veprek, Appl. Phys. Lett. 91 (2007) 031906.
[34] F. Birch, Phys. Rev. 71 (1947) 809.
[35] H. He, T. Sekine, T. Kobayashi, H. Hirosaki, I. Suzuki, Phys. Rev. B 62 (2000) 11412.
[36] E. Soignard, M. Somayazulu, J.J. Dong, O.F. Sankey, P.F. McMillan, J. Phys.: Condens. Matter 13 (2001) 575.
[37] C. Kocer, N. Hirosaki, S. Ogata, Phys. Rev. B 67 (2003) 035210.
[38] R. Hill, Proc. Phys. Soc. Lond. A 65 (1952) 349.
[39] M. Born, Proc. Cambridge Philos. Soc. 36 (1940) 160.
[40] A.S. Argon, Topics in Fracture and Fatigue, Springer, New York, 1992.
[41] G. Xu, A.S. Argon, M. Ortiz, Philos. Mag. A 75 (1997) 341.
[42] S.F. Pugh, Philos. Mag. 45 (1954) 823.
[43] A. Cazzani, M. Rovati, Int. J. Solids Struct. 40 (2003) 1713.
[44] J.F. Nye, Physical Properties of Crystals: Their Representation by Tensors and Matrices, Oxford University Press, New York, 1985.
[45] R.F. Zhang, S. Veprek, A.S. Argon, Phys. Rev. B 77 (2008) 172103.
[46] R.F. Zhang, Z.J. Lin, S. Veprek, Phys. Rev. B 83 (2011) 155452.